DOI:
10.1038/nnano.2012.212

Document Version
Peer reviewed version

Published in final edited form as:
Nat Nanotechnol. 2013 January ; 8(1): 61–68. doi:10.1038/nnano.2012.212.

Biomimetic functionalization with leukocyte membranes imparts cell like functions to synthetic particles

Alessandro Parodi[1,2,‡], **Nicoletta Quattrocchi**[1,3,‡], **Anne L. van de Ven**[1], **Ciro Chiappini**[1,†], **Michael Evangelopoulos**[1], **Jonathan O. Martinez**[1,4], **Brandon S. Brown**[1,4], **Sm Z. Khaled**[1], **Iman K. Yazdi**[1,5], **Maria Vittoria Enzo**[1,6], **Lucas Isenhart**[1], **Mauro Ferrari**[1], and **Ennio Tasciotti**[1]

[1]Department of Nanomedicine, The Methodist Hospital System Research Institute, Houston, TX 77030, USA

[2]Department of Experimental Oncology and Molecular Medicine, Fondazione IRCCS Istituto Nazionale Tumori, Milan 20133, Italy

[3]Department of Experimental Medicine, University of Milano Bicocca, Milan 20052, Italy

[4]The University of Texas Health Science Center at Houston, Houston, TX 77030, USA

[5]Department of Biomedical Engineering, University of Houston, Houston, TX 77204, USA

[6]Department of Oncological and Surgical Sciences, 2nd Surgical Clinic, University of Padua, Padua 35128, Italy

Abstract

The therapeutic efficacy of systemic drug delivery vehicles depends on their ability to evade the immune system, cross the biological barriers of the body and localize at target tissues. Leukocytes possess all of these functions and exert their targeting ability through cellular membrane interactions. Here we show that NanoPorous Silicon particles (NPS) can successfully perform all these actions when coated with cellular membranes purified from white blood cells. These hybrid particles called LeukoLike Vectors (LLV) were able to: prevent rapid clearance of phagocytic cells of the immune system; communicate with endothelial cells through receptor-ligand interaction; transport and release a payload across an inflamed reconstructed endothelium. Furthermore, LLV retained their functions when injected *in vivo*, showing enhanced circulation time and improved accumulation in the tumour.

Correspondence to: Ennio Tasciotti.
†Current address: Department of Materials, Imperial College London.
‡These authors contributed equally to this work.

Supplementary information accompanies this paper at www.nature.com/naturenanotechnology.

The authors declare competing financial interests.

Authors' Contribution Statement.
A. P. supervised all cellular experiments, interpreted the data and wrote the manuscript; N. Q. developed and optimized protocols Leukolike Vector assembly; A.V. designed and performed all intravital microscopy experiments and analysis and wrote the paper; C. C. manufactured the NPS; M.E. optimized the development of the system; J.O.M. carried out and analysed time-lapse microscopy experiments; B.B. performed confocal microscopy and flow cytometry; S. K. performed the physical and chemical characterization; I. K. Y. performed SEM and assisted with analysis; M.V.E. performed the transwell assays; L.I. optimized in vitro flow systems; M. F. performed the final edits of the manuscript and mentored the authors during the development of the project; E. T. conceived the LLV concept, wrote the paper and was the PI of the major supporting grants.

Biophysical barriers protect the body by regulating the trafficking, exchange, and clearance of foreign materials [1]. For example, endothelial cells of blood vessels are responsible for identifying and capturing potential hazards [2]. Upon entering the blood, systemically injected drugs and particles are tagged with proteins (a process called opsonisation[3]) for subsequent removal by the body's immune system known as the mononuclear phagocyte system [4]. Therefore, to function properly, systemic agents must avoid clearance by the immune system, negotiate past the vascular barrier, and localize at the target tissue in sufficient quantities [5].

Encapsulating free drugs in nanoparticles is advantageous because it prolongs the drug half-life, improves its site-specific targeting, reduces side-effects and enhances therapeutic efficacy without requiring alterations to the chemistry of the drug [6–8]. Moreover, the physical and chemical properties of the nanoparticles themselves confer new capabilities *in vivo* [9, 10]. For example, optimization of particles' size [11, 12], shape [13], and surface charge [14], enhance passive tumour targeting via a mechanism known as enhanced permeation and retention [15]. Furthermore, modification of the surfaces of particles with polyethylene glycol (PEG) improves biodistribution of chemotherapeutics [16], while bioconjugation of active targeting molecules enhances delivery to specific cells [17, 18]. More recently, efforts have focused on the development of multistage vectors that decouple each of these functions *in vivo* [19]. Based around a NanoPorous Silicon (NPS) platform [18, 20], these particles can carry a variety of cargoes[20–22], navigate through blood flow [21, 23], recognize and bind specific endothelial targets[23, 24], and protect therapeutic cargo for enhanced efficacy[22, 25].

Yet, particle-based drug delivery has not reached its full therapeutic potential [21, 26]. Avoiding opsonization and non-specific clearance remains a challenge [27] and the use of PEG can not completely prevent clearance [28] and eventually activate the human complement system [29]. Particles with longer circulation times have shown increase probability of tumoritropic accumulation in tumours with fenestrated endothelia [30, 31]. Regrettably, not all tumors are characterized by increased vessel permeability. Under these circumstances, the use of current delivery systems is highly ineffective and the negotiation of the vascular barriers is a mandatory step to attain the desired drug biodistribution and acceptable therapeutic indices.

Given the complexity of mass transport in vascular compartment, it is not surprising that "biomimetic camouflage" strategies are gaining popularity [32, 33]. Virus-based carriers [34], targeted protocells [35], and bio-nano hybrid systems[36, 37] have been proposed as potential strategies for overcoming vascular barriers to drug delivery. Here we describe an approach to transfer bioactive cellular components to the surface of synthetic particles in order to confer unique functions not otherwise attainable through current bioconjugation techniques. This new generation of injectable carriers, named LeukoLike Vectors (LLV), are produced by camouflaging NPS particles with cellular membranes isolated from freshly harvested leukocytes. Using a combination of *in vitro* and *in vivo* experiments, we show that LLV are able to avoid opsonisation, delay uptake by the mononuclear phagocyte system, preferentially bind inflamed endothelium, and facilitate chemotherapeutics transport across the endothelium while eluding the lysosomal pathway.

Assembly and characterization

LLV were produced by cloaking NPS with cellular membranes isolated from freshly harvested leukocytes (Figure 1A). The membranes were purified by ultracentrifugation through a discontinuous sucrose density gradient (Supplementary figure S2), and reconstituted as proteo-lipid patches. Self-assembly of the LLV was driven by electrostatic and hydrophobic interactions between the negatively charged proteo-lipid patches and the

positively charged NPS surface (Figure 1B). As a result, the zeta potential of the (3-aminopropyl)triethoxysilane (APTES) modified NPS surface switched from +7.41 mV to a negative value similar to that of leukocytes (LLV: −26 mV, Leukocytes: −31.16 mV) (Supplementary table 1). Fourier transform infrared spectroscopy (Supplementary figure S3) suggested that the system was at least partially stabilized by amide bonds between the carboxylic groups of the proteo-lipids and amine groups on the NPS surface (Figure 1C). The lipid: particle ratio and vesicle lamellarity was varied to modulate the uniformity, thickness, and surface stability of the coating (Figure 1D–F). Fusion between adjacent proteo-lipid patches and lipid vesicles resulted in complete coverage of the particle surface (Figure 1G–I). The resulting LLV appeared to retain critical leukocyte transmembrane proteins in the same orientation as their donor cells. Both CD45 and CD3z, two biomarkers expressed on the membrane of leukocytes [38], and Lymphocyte Function-associated Antigen 1 (LFA-1 or CD11a), an adhesion molecule utilized by leukocytes for vascular extravasation [39–41], were confirmed to be exposed on the LLV surface using immunoblotting and flow cytometry (Supplementary figure S2, S4). LLV composition and stability were evaluated over time through thermogravimetric analysis and scanning electron microscopy (SEM) (Supplementary figure S5–6). After 24 hours, more than half of the membrane coating remained associated with the particles, resulting in delayed particle degradation and cargo release kinetics (Supplementary figure S7).

Inhibition of particle opsonization and reduced phagocytosis

The LLV surface was stained for sialic acid and N-acetylglucosamine glycans, two typical post-transcriptional modifications of transmembrane proteins that play a key role in the cellular self-recognition mechanisms[42]. Their presence was quantified by spectrofluorimetric quantification of wheat germ agglutinin absorption on the NPS and LLV surface (Figure 2A). The LLV coating was found to also protect the particle surface from opsonization by highly abundant serum proteins. LLV incubated with fluorescent IgG and bovine serum albumin demonstrated significantly less (~10-fold decrease) protein absorption than NPS (Figure 2B–C).

The ability of the LLV coating to inhibit particle internalization was studied using murine J774 macrophages and human THP-1 phagocytic cells. Both cell lines were individually incubated with equivalent numbers of fluorescently labelled NPS and LLV particles coated with the membranes of each cell type. Particle internalization was quantified using flow cytometry three hours after treatment (Figure 2D–E). The LLV coating was found to significantly decrease particle uptake, particularly when the donor membrane matched that of the host phagocytic cell. Particles coated with J774 membranes showed a ~75% decrease in uptake by J774 cells whereas particles coated with THP-1 membranes showed a ~50% decrease in uptake by THP-1 cells. Mismatch between the donor and host cells instead led to a limited decrease in uptake (~50% for THP-1 LLV and ~10% for J774 LLV). These trends were also observed using Time Lapse Microscopy (TLM) (Supplementary figure S8, Supplementary movies 1–6,). No significant impact on cell viability or particle toxicity was observed following LLV treatment (Supplementary figure S9). This evidence suggests that the particle opsonization and the consequent specific clearance are inhibited by the membrane coating and that the source of the cellular membrane can affect the rate of internalization, depending on the experimental model used.

Vascular intra and intercellular trafficking of LLV

The interaction of LLV with a confluent monolayer of human umbilical vein endothelial cells (HUVEC) was studied using NPS particles coated with Jurkat cell membranes, henceforth simply referred to as LLV. As previously reported [43], early NPS internalization

(~15 min) was characterized by the formation of filopodia "cages" that surrounded and locked particles against the cell surface. While untreated endothelium appeared smooth and regular under SEM (Supplementary figure S10), NPS-treated endothelium showed several irregularities, including the formation of membrane protrusions and abundant outward vesicle budding (Figure 3A). In contrast, LLV treatment did not induce any notable change in the cell membranes and LLV internalization involved neither filopodia nor vesicle formation (Figure 3A). Differences remained after complete particle uptake (~60 min), with NPS particles still recognizable immediately below the cell surface while the cells displayed several ring-like structures in association with LLV internalization events (Figure 3A).

Immunostaining of LLV surface revealed a punctate and regularly spaced distribution of LFA-1 across the particle (Supplementary Figure 11). We postulated that LFA-1 would play an important role in LLV recognition of and binding to inflamed endothelium. The ability of LLV to recruit LFA-1 receptor ICAM-1, a cell adhesion molecule over-expressed following TNF-α stimulation[44], was studied under physiological flow using an inflamed endothelium model (Figure 3B). LLV adhering to the endothelial surface were able to locally induce clustering of ICAM-1. In contrast, ICAM-1 was homogenously distributed before LLV administration or following NPS administration. ICAM-1 clustering was inhibited by pre-treating LLV with an antibody against the active site of LFA-1. Typical clustering events between ICAM-1 and LLV are shown in the rainbow colour insets (Figure 3B). LLV and NPS also displayed markedly different adhesion to healthy and inflamed endothelial cell monolayers under flow (Figure 3C). Under both normal and inflamed conditions, NPS showed a high quantity of binding to endothelium whereas LLV doubled their binding upon HUVEC pre-treatment with TNF-α. The increase in LLV binding appeared to be mediated by LFA-1, since its blockage by an antibody reduced LLV binding to the endothelium.

Confocal microscopy studies performed during LLV and NPS internalization revealed local rearrangements of the cytoskeleton around LLV, whereas NPS failed to alter the architecture and distribution of actin filaments (Figure 3D–E). Interestingly, actin filaments surrounding LLV appeared to be organized in a channel-like formation. Three-dimensional confocal z-stacks demonstrated "basket-like structures" protruding from the basal side of the cell and associated with the LLV (Supplementary movies S7–8). The subcellular localization of LLV and NPS was analysed by TEM for up to 24 hours, demonstrating that internalized LLV were able to avoid lysosomal sequestration (Figure 3F and Supplementary figure S12–13). LLV appeared to retain their leukocyte coating (see black arrow in the right inset) and were in direct contact with the cell cytoplasm, whereas NPS remained trapped inside the endolysosomal compartment (see black arrow in the left inset) and were trafficked toward the perinuclear region as previously described[45].

The ability of LLV to cross a reconstructed endothelial monolayer was studied *in vitro* using a transwell system (Figure 4A) under physiologic and inflammatory conditions. LLV and NPS were added to a confluent HUVEC monolayer for 3 hours, in the presence and absence of TNF-α. Particle distribution was evaluated in the three compartments that characterize a transwell system: free particles in upper chamber, entrapped particles in the endothelial monolayer and particles transported through the monolayer and recovered in the lower chamber (Figure 4B, Supplementary figure S14). Under normal conditions (no TNF-α), the quantity of LLV recovered from the upper chamber was significantly higher than the quantity of NPS recovered (~25% vs. ~5% respectively). Only a small percentage of both particle types migrated to the other side of the filter; instead ~75% of LLV and ~90% of NPS were found inside endothelial cells. In the presence of TNF-α, the quantity of LLV recovered from the bottom chamber increased significantly from ~2% to ~70%. A relative decrease in the number of particles found in the supernatant and intracellular compartments accompanied this change. NPS transport increased to a lesser degree, from ~2% to ~30%,

with >50% of NPS remaining in the intracellular compartment. This data showed that in the presence of inflamed conditions, the membrane coating increases particle transportation through an endothelium monolayer, thereby increasing the permeability of this biological barrier.

The ability of LLV to increase the permeability of inflamed HUVEC monolayers was measured assessing the transendothelial electrical resistance (TEER). Compared to NPS, the treatment of the endothelial monolayers with LLV resulted in a transient drop in resistance. The maximal drop occurred after 20 minutes of incubation, yielding a ~35% drop in TEER (Figure 4C). No significant change in TEER was observed with NPS addition, suggesting that the ~4-fold relative difference between LLV and NPS transport is mediated by the biomimetic coating.

The therapeutic potential of LLV was assessed using a similar transwell model comprised of a confluent HUVEC monolayer in the upper chamber and a confluent MDA-MB-231 breast cancer cell monolayer in the bottom chamber. Particles were loaded with Doxorubicin (DOX), and the cytotoxic activity of DOX-loaded particles was compared to that of free DOX 48 hours after treatment (Figure 4D). Both free DOX and DOX-NPS had little effect on tumour cell viability, reducing MDA-MB-231 viability by ~20% and ~10% respectively. Most of the DOX-induced cytotoxic effect was observed in the endothelial cell layer, whose viability was reduced by ~73% and ~71% respectively. In contrast, LLV reduced cancer cell viability by ~57% while maintaining more than ~80% of the endothelial layer's viability. Taken together, this data suggest that LLV can successfully transport the DOX payload through the endothelium and effectively release it in the lower chamber.

Delayed liver clearance and tumour accumulation in mice

The ability of LLV to evade the mononuclear phagocyte system and accumulate within tumours *in vivo* was quantified by tracking individual particles using intravital microscopy. Systemically administered murine-derived J774 LLV showed delayed accumulation in the liver, indicating that the integrity of the biomimetic camouflage is retained for up to 40 minutes *in vivo* (Figure 5A). This time-dependent accumulation was largely mediated by phagocytic Kupffer cells; however, we observed a statistically significant subset of adherent LLV ($p<0.05$) which was not internalized by Kupffer cells (Figure 5B). These non-phagocytized LLV (~25% of adherent LLV) were generally associated with the liver endothelium (Figure 5C, arrows) rather than the surface of Kupffer cells. The tumoritropic accumulation of LLV in mice inoculated with murine B16 melanoma was enhanced compared to that of NPS (Figure 5D). Particle coating using leukocyte membranes led to a ~2-fold increase in particle density at the tumour across all mice examined. Competition experiments of differentially labelled particles (Figure 5E, 5F) showed that LLV and NPS adhered to the tumour endothelium in a time-dependent manner.

Conclusions

The development of efficient systemic drug delivery vehicles requires evasion of the mononuclear phagocyte system, preferential localization to the target organ, and negotiation past the endothelial barrier. These properties are crucial for delivering therapeutic quantities of drug to the tissue of interest [26, 31, 46]. In this study, we showed that leukocyte-based biomimetic camouflage was able to provide a competitive advantage for overcoming sequential vascular barriers by reducing opsonisation, leveraging self-recognition mechanisms to delay phagocytic uptake, binding inflamed endothelium, and facilitating transport across the endothelial layer while eluding the lysosomal pathway. Furthermore, LLV appeared sufficiently stable *in vivo* to enhance particle circulation time and improve

tumoritropic accumulation. Taken together, these results suggest that LLV may be well suited for chemotherapeutics delivery to cancer.

Unlike conventional nanocarriers, which rely on passive enhanced permeation and retention effects to accumulate in tumours [31, 47], LLV have the potential to recognize and bind tumour endothelium in an active, non-destructive manner. It is intriguing to contemplate that future tumoritropic drug carriers will avoid the need for fenestrated endothelium[48] and alleviate concerns regarding particle-induced injury to endothelial barrier function[49]. While additional studies will follow to address LLV stability, immunogenicity, transport, and pharmacokinetics *in vivo,* this proof-of-concept study demonstrates that it is possible to successfully transfer bioactive cellular components to a synthetic system in order to improve the negotiation of vascular barriers.

Materials and Methods

Cell Culture

Jurkat, THP-1, J774, HUVEC and MDA-MB-231 cell lines were purchased from the American Type Culture Collection (ATCC; US) and cultured according to the vendor directions. HUVEC were used within the first 10 passages of culture and stimulated with TNF-α (10 ng/ml) (e-Bioscience) for 24 hours before co-incubation with particles. In all the experiments, the particle: cell ratio was 5:1, unless otherwise indicated.

Leukolike Vector Assembly

NPS of 3.2 μm diameter, functionalized with APTES, were incubated with leukocyte proteo-lipid membranes as described in the Supplementary Information. Chemical and physical particle analysis and drug loading/release, are described there as well.

Confocal Microscopy

HUVEC were seeded at 75,000 cells/filter on ThinCerts™ inserts (8 μm pore size) coated with fibronectin and co-incubated with NPS or Jurkat LLV (tagged with PE-Rhod and DyLight 488 respectively) for 3 hours. After treatment, cells were fixed and stained for actin using Alexa Fluor 594-phalloidin as described in Serda et al. HUVEC cell monolayers treated with NPS and Jurkat LLV under flow (see below) were stained for ICAM-1 expression using anti-ICAM-1 (Abcam) followed by IgG-488 (Invitrogen). Images were acquired using an upright Leica DM6000 or inverted Nikon A1 confocal microscope equipped with spectral detector and 63x oil-immersion objective. Fluorescence line intensity profiles and topographic intensity plots of ICAM-1 clustering were analysed using Nikon Elements v3.2 to distinguish between free, adherent, and internalized particles. Particle counts were performed manually using high-resolution image mosaics of the entire slide. Zeta-stacks, collected at 0.7μm intervals, were deconvoluted using AutoQuant Blind Deconvolution within Nikon Elements. 3D reconstructions and movies were prepared using the same software.

Endothelial Permeability Assessment

HUVEC were seeded at 80,000 cells/filter on ThinCerts™ inserts coated with fibronectin (10mg/ml) and co-incubated with NPS or Jurkat LLV at a particle: cell ratio of 2:1 for 3 hours. For each experiment, 6 replicates were performed in addition to 2 controls without cells. After incubation, the media was collected from each chamber. Lower chambers were washed with PBS and scraped twice to recover all particles. The filters with adhering cells were rinsed twice with PBS. Collected particles were centrifuged, resuspended in PBS, and spotted on 8-chamber slides. The number of particles was estimated by counting 5 randomly selected fields (20x magnification) under wide-field fluorescence using a Nikon TiE

inverted microscope. The total number of particles was calculated by multiplying the number of particles in the observed field by the number of fields within the total area. The number of filtered LLV was adjusted relative to the cell-free control to correct for particle entrapment in the filter itself (supplementary figure 14). For the assessment of the payload transport, transwell chambers were prepared as described above. MDA-MB-231 cells were cultured at a density of 60% on the lower chamber. Particles were added to the upper chamber at a particle: cell ratio of 5:1 for 48 hours, after which cell viability was assayed using an MTT assay as recommended by vendor instructions.

Trans Endothelial Electrical Resistance (TEER) Measurement

The TEER of confluent HUVEC monolayers (seeded as previously described) was measured at 20-minute intervals before and after particle addition (20 particles/cell) using an EVOM2 voltmeter (World Precision Instruments).

Animal models

Transgenic Tie2-GFP mice (Jackson Labs) and wild-type C57BL/6J mice (Charles River Laboratories) were utilized for all *in vivo* studies. Melanoma tumours were generated in the flank of C57BL/6J mice by a one-time subcutaneous injection of 10^6 murine B16 cells. The tumour vasculature was delineated by a one-time injection of 40kDa FITC-dextran tracer (Invitrogen). Three days prior to imaging, Tie-2 GFP+ mice received a one-time injection of DiD-labeled autologous red blood cells[23] to label Kupffer cells. All animal protocols were reviewed and approved by the IACUC at The Methodist Hospital Research Institute.

Intravital Microscopy (IVM)

In vivo particle dynamics were imaged in real-time as described in[50] using a Nikon A1R laser scanning confocal microscope adapted for IVM[50]. Isoflurane anesthetized mice were surgically prepared as in[50], intravenously treated one or two doses of 0.5×10^7 particles in 50 μl PBS, and monitored for up to 3 hours. Particle accumulation and phagocytosis was quantified using Image J v1.45 (NIH) and NIS Elements v4.1 as in[50].

Statistical Analysis

All the data are the result of a minimum of three independent experiments. Statistics were calculated with Prism GraphPad software (LaJOlla, California, USA). The significance was calculated through OneWay Anova method, followed by Dunnett's test or with independent Student's T-Test.

Supplementary Material

Refer to Web version on PubMed Central for supplementary material.

Acknowledgments

The authors acknowledge the Alliance for NanoHealth Department of Defence Telemedicine & Advanced Technology Research Center 09 - W81XWH-10-2-0125; Defense Advanced Research Projects Agency - W911NF-11-1-0266; National Institute of Health U54CA143837 and U54CA151668, Department of Defense/ Breast Cancer Research Program (W81XWH-09-1-0212); N. Q. was supported from Ministero Istruzione Universita Ricerca, Italy; A. P. was supported from the Bianca Garavaglia Association, (Busto Arsizio, Varese, Italy); J.O.M. was supported by the National Institute of Health Center for Clinical and Translational Sciences, Clinical and Translational Award TL1 RR024147 from the National Center for Research Resources; M. V. E. was supported by Euroclone S.p.a. The content is solely the responsibility of the authors and does not necessarily represent the official views of the National Center for Research Resources or the National Institutes of Health.

The authors thank Masserini M. E., Agostini M. Nitti D. and Hussain F. for their mentoring role, Liu X. for the fabrication of the nanoporous silicon particles, Dunner K. Jr. for the assistance with transmission electron

microscopy, Cui K. and The Methodist Hospital Research Institute Advanced Cellular and Tissue Microscope Core Facility for time-lapse live cell microscopy, Haviland D. and The Methodist Hospital Research Institute Flow Cytometry Core Facility and De Rosa E. for data analysis, Warier N., Scaria S., Adriani G., Decuzzi P., Zabre E. V. and Grattoni A. for technical support and Landry M. G. for graphical assistance.

References

1. Bauer HC, et al. New aspects of the molecular constituents of tissue barriers. J Neural Transm. 2011; 118:7–21. [PubMed: 20865434]
2. Rabanel JM, Aoun V, Elkin I, Mokhtar M, Hildgen P. Drug-loaded nanocarriers: Passive targeting and crossing of biological barriers. Curr Med Chem. 2012; 19:3070–3102. [PubMed: 22612696]
3. Owens DE 3rd, Peppas NA. Opsonization, biodistribution, and pharmacokinetics of polymeric nanoparticles. Int J Pharm. 2006; 307:93–102. [PubMed: 16303268]
4. Moghimi SM, Davis SS. Innovations in avoiding particle clearance from blood by kupffer cells: Cause for reflection. Crit Rev Ther Drug Carrier Syst. 1994; 11:31–59. [PubMed: 7704918]
5. Jain RK. Delivery of molecular and cellular medicine to solid tumors. Adv Drug Deliv Rev. 2001; 46:149–168. [PubMed: 11259838]
6. Torchilin VP. Recent advances with liposomes as pharmaceutical carriers. Nature Reviews Drug Discovery. 2005; 4:145–160.
7. Banerjee S, Li Y, Wang Z, Sarkar FH. Multi-targeted therapy of cancer by genistein. Cancer Lett. 2008; 269:226–242. [PubMed: 18492603]
8. Davis ME, Chen ZG, Shin DM. Nanoparticle therapeutics: An emerging treatment modality for cancer. Nat Rev Drug Discov. 2008; 7:771–782. [PubMed: 18758474]
9. Barreto JA, et al. Nanomaterials: Applications in cancer imaging and therapy. Adv Mater. 2011; 23:H18–40. [PubMed: 21433100]
10. Mitragotri S, Lahann J. Physical approaches to biomaterial design. Nat Mater. 2009; 8:15–23. [PubMed: 19096389]
11. Yuan F, et al. Microvascular permeability and interstitial penetration of sterically stabilized (stealth) liposomes in a human tumor xenograft. Cancer Res. 1994; 54:3352–3356. [PubMed: 8012948]
12. Yuan F, et al. Vascular permeability in a human tumor xenograft: Molecular size dependence and cutoff size. Cancer Res. 1995; 55:3752–3756. [PubMed: 7641188]
13. Champion JA, Katare YK, Mitragotri S. Particle shape: A new design parameter for micro- and nanoscale drug delivery carriers. J Control Release. 2007; 121:3–9. [PubMed: 17544538]
14. Campbell RB, et al. Cationic charge determines the distribution of liposomes between the vascular and extravascular compartments of tumors. Cancer Res. 2002; 62:6831–6836. [PubMed: 12460895]
15. Matsumura Y, Maeda H. A new concept for macromolecular therapeutics in cancer chemotherapy: Mechanism of tumoritropic accumulation of proteins and the antitumor agent smancs. Cancer Res. 1986; 46:6387–6392. [PubMed: 2946403]
16. Cho YI, Park S, Jeong SY, Yoo HS. In vivo and in vitro anti-cancer activity of thermo-sensitive and photo-crosslinkable doxorubicin hydrogels composed of chitosan–doxorubicin conjugates. Eur J Pharmaceut Biopharmaceut. 2009; 73:59–65.
17. Albrecht H. Trastuzumab (herceptin(r)): Overcoming resistance in her2-overexpressing breast cancer models. Immunotherapy. 2010; 2:795–798. [PubMed: 21091112]
18. Chiappini C, et al. Tailored porous silicon microparticles: Fabrication and properties. Chemphyschem. 2010; 11:1029–1035. [PubMed: 20162656]
19. Godin B, Tasciotti E, Liu X, Serda RE, Ferrari M. Multistage nanovectors: From concept to novel imaging contrast agents and therapeutics. Acc Chem Res. 2011; 44:979–989. [PubMed: 21902173]
20. Tasciotti E, et al. Mesoporous silicon particles as a multistage delivery system for imaging and therapeutic applications. Nat Nanotechnol. 2008; 3:151–157. [PubMed: 18654487]
21. Ananta JS, et al. Geometrical confinement of gadolinium-based contrast agents in nanoporous particles enhances t1 contrast. Nat Nanotechnol. 2010; 5:815–821. [PubMed: 20972435]

22. Tanaka T, et al. Nanotechnology for breast cancer therapy. Biomed Microdevices. 2009; 11:49–63. [PubMed: 18663578]
23. van de Ven AL, et al. Rapid tumoritropic accumulation of systemically injected plateloid particles and their biodistribution. J Control Release. 2012; 158:148–155. [PubMed: 22062689]
24. Mann AP, et al. E-selectin-targeted porous silicon particle for nanoparticle delivery to the bone marrow. Adv Mater. 2011; 23:278–282.
25. Shen H, et al. Cancer therapy: Cooperative, nanoparticle-enabled thermal therapy of breast cancer. Adv Healthcare Mater. 2012; 1:128–128.
26. Michor F, Liphardt J, Ferrari M, Widom J. What does physics have to do with cancer? Nat Rev Cancer. 2011; 11:657–670. [PubMed: 21850037]
27. Moghimi SM, Szebeni J. Stealth liposomes and long circulating nanoparticles: Critical issues in pharmacokinetics, opsonization and protein-binding properties. Prog Lipid Res. 2003; 42:463–478. [PubMed: 14559067]
28. Immordino ML, Dosio F, Cattel L. Stealth liposomes: Review of the basic science, rationale, and clinical applications, existing and potential. Int J Nanomed. 2006; 1:297–315.
29. Gabizon, AA.; FMM. Long circulating liposomes: Old drugs, new therapeutics. Springer-Verlag and Landes Bioscience; 1998.
30. Maeda H, Wu J, Sawa T, Matsumura Y, Hori K. Tumor vascular permeability and the epr effect in macromolecular therapeutics: A review. J Control Release. 2000; 65:271–284. [PubMed: 10699287]
31. Torchilin V. Tumor delivery of macromolecular drugs based on the epr effect. Adv Drug Deliv Rev. 2011; 63:131–135. [PubMed: 20304019]
32. Yoo JW, Irvine DJ, Discher DE, Mitragotri S. Bio-inspired, bioengineered and biomimetic drug delivery carriers. Nat Rev Drug Discov. 2011; 10:521–535. [PubMed: 21720407]
33. Barenholz Y. Sphingomyelin and cholesterol: From membrane biophysics and rafts to potential medical applications. Subcell Biochem. 2004; 37:167–215. [PubMed: 15376621]
34. Manchester M, Singh P. Virus-based nanoparticles (vnps): Platform technologies for diagnostic imaging. Adv Drug Deliv Rev. 2006; 58:1505–1522. [PubMed: 17118484]
35. Ashley CE, et al. The targeted delivery of multicomponent cargos to cancer cells by nanoporous particle-supported lipid bilayers. Nat Mater. 2011; 10:389–397. [PubMed: 21499315]
36. Merkel TJ, et al. Using mechanobiological mimicry of red blood cells to extend circulation times of hydrogel microparticles. Proc Natl Acad Sci. 2011; 108:586–591. [PubMed: 21220299]
37. von Maltzahn G, et al. Nanoparticles that communicate in vivo to amplify tumour targeting. Nat Mater. 2011; 10:545–552. [PubMed: 21685903]
38. van Vliet SJ, Gringhuis SI, Geijtenbeek TB, van Kooyk Y. Regulation of effector t cells by antigen-presenting cells via interaction of the c-type lectin mgl with cd45. Nat Immunol. 2006; 7:1200–1208. [PubMed: 16998493]
39. Carman CV. Mechanisms for transcellular diapedesis: Probing and pathfinding by ‘invadosome-like protrusions’. J Cell Sci. 2009; 122:3025–3035. [PubMed: 19692589]
40. Millan J, et al. Lymphocyte transcellular migration occurs through recruitment of endothelial icam-1 to caveola- and f-actin-rich domains. Nat Cell Biol. 2006; 8:113–123. [PubMed: 16429128]
41. Yang L. Icam-1 regulates neutrophil adhesion and transcellular migration of tnf-a-activated vascular endothelium under flow. Blood. 2005; 106:584–592. [PubMed: 15811956]
42. Rebman B. Tumor immunology. ACP Medicine. 2011; 206:137–151.
43. Serda RE, et al. Mitotic trafficking of silicon microparticles. Nanoscale. 2009; 1:250–259. [PubMed: 20644846]
44. Barreiro O, et al. Dynamic interaction of vcam-1 and icam-1 with moesin and ezrin in a novel endothelial docking structure for adherent leukocytes. J Cell Biol. 2002; 157:1233–1245. [PubMed: 12082081]
45. Ferrati S, et al. Intracellular trafficking of silicon particles and logic-embedded vectors. Nanoscale. 2010; 2:1512–1520. [PubMed: 20820744]

46. Ferrari M. Frontiers in cancer nanomedicine: Directing mass transport through biological barriers. Trends Biotechnol. 2010; 28:181–188. [PubMed: 20079548]

47. Petros RA, DeSimone JM. Strategies in the design of nanoparticles for therapeutic applications. Nat Rev Drug Discov. 2010; 9:615–627. [PubMed: 20616808]

48. Taurin S, Nehoff H, Greish K. Anticancer nanomedicine and tumor vascular permeability; where is the missing link? J Control Release. 2012

49. Trickler WJ, et al. Silver nanoparticle induced blood-brain barrier inflammation and increased permeability in primary rat brain microvessel endothelial cells. Toxicol Sci. 2010; 118:160–170. [PubMed: 20713472]

50. van de Ven AL, et al. Integrated intravital microscopy and mathematical modeling to optimize nanotherapeutics delivery to tumors. AIP Adv. 2012; 2:11208. [PubMed: 22489278]

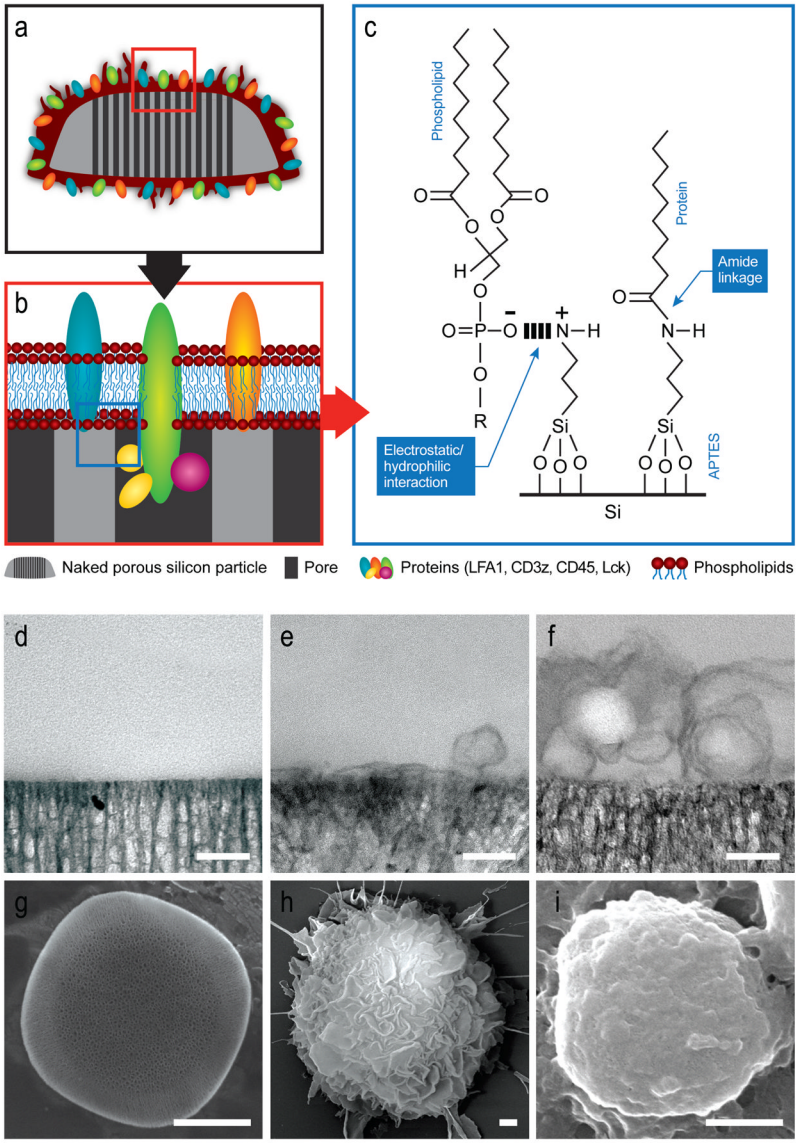

Figure 1. The LeukoLike Vector

a, A cartoon of LLV: the leukocyte-derived cell membranes fully cover the NPS and seal off its pores. **b**, Zoom-in of red box in a. Schematic showing relevant proteins (LFA-1, CD3z, CD45, Lck) in the membrane are interspersed in the porous structure of the NPS. **c,** Schematic showing the interactions between the APTES group on the NPS surface and a membrane phospholipid (left) and protein (right). Phosphate groups on the phospholipid form electrostatic/hydrophilic interactions, whereas carboxylic groups of proteins can form amide bonds. **d**, Transmission electron micrograph (TEM) of bare NPS reveal the open pores. **e**, In the presence of unilamellar vesicles, LLV coating thickness is similar to that of normal lipid bilayers. **f**, The coating can reach thicknesses up to 500 nm depending on the number of membrane layers and the extent of their fusion to the NPS. **g–i**, Scanning electron micrograph (SEM) of a bare NPS surface (**g**), a leukocyte used as a membrane donor (**h**), and an NPS camouflaged with leukocyte-derived membranes (**i**), which appears similar to h. Scale bars = 100 nm (TEM), 1 μm (SEM).

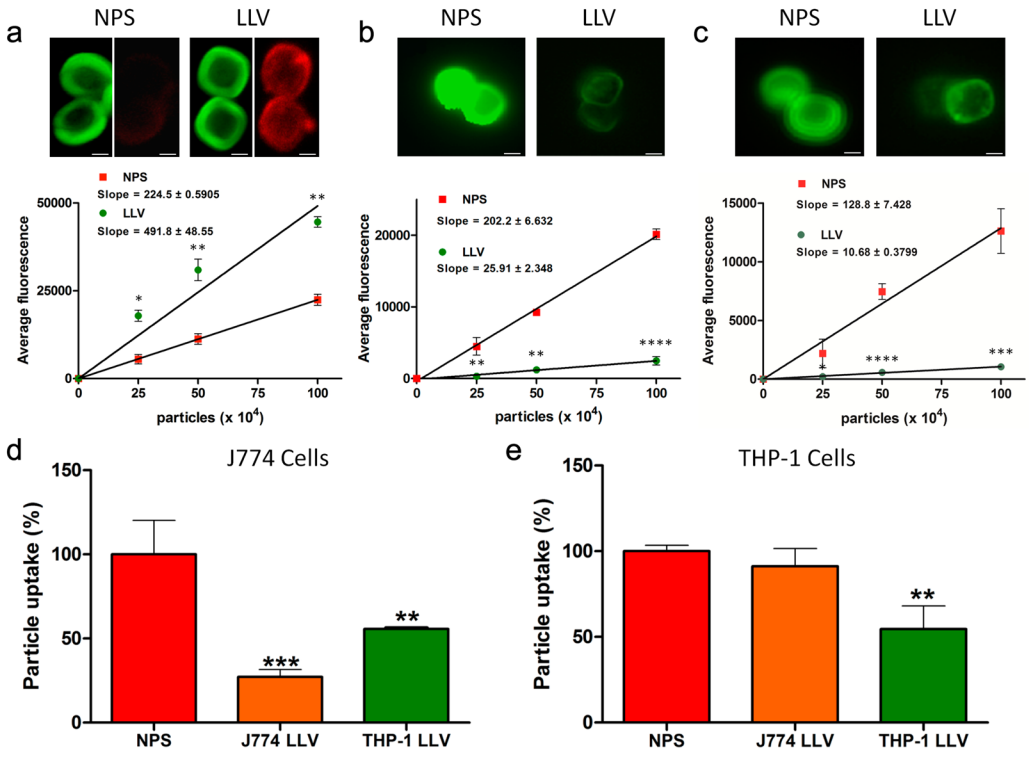

Figure 2. Inhibition of particle opsonization and phagocytosis

a, Staining of the LLV (green box) and NPS (red box) particles using wheat germ agglutinin (particles on right of each box, red) to reveal N-acetylglucosamine and sialic acid groups on the surface of the NPS and LLV (particles on left of each box, green). Scale bars = 1μm. Fluorometric quantification demonstrates enhanced LLV staining in the graph below. **b,** Differential opsonization by passive absorption of IgG (green, both boxes) to the surface of NPS (left, red box) and LLV (right, green box). Scale bars = 1 μm. Quantification displayed in the graph below. **c,** Albumin (green) absorbs passively to the surface of NPS (left, red box) and LLV (right, green box). Scale bars = 2μm. Fluorometric analysis reveals the slope of fluorescence vs particle concentration in the graph below **d–e,** Internalization of particles by J774 (d) and THP-1 (e) with coatings derived from either cell line, measured by flow cytometry following 3hr co-incubation. Values and significance are expressed as relative to NPS treated cells. ** = $p < 0.01$, *** = $p < 0.001$.

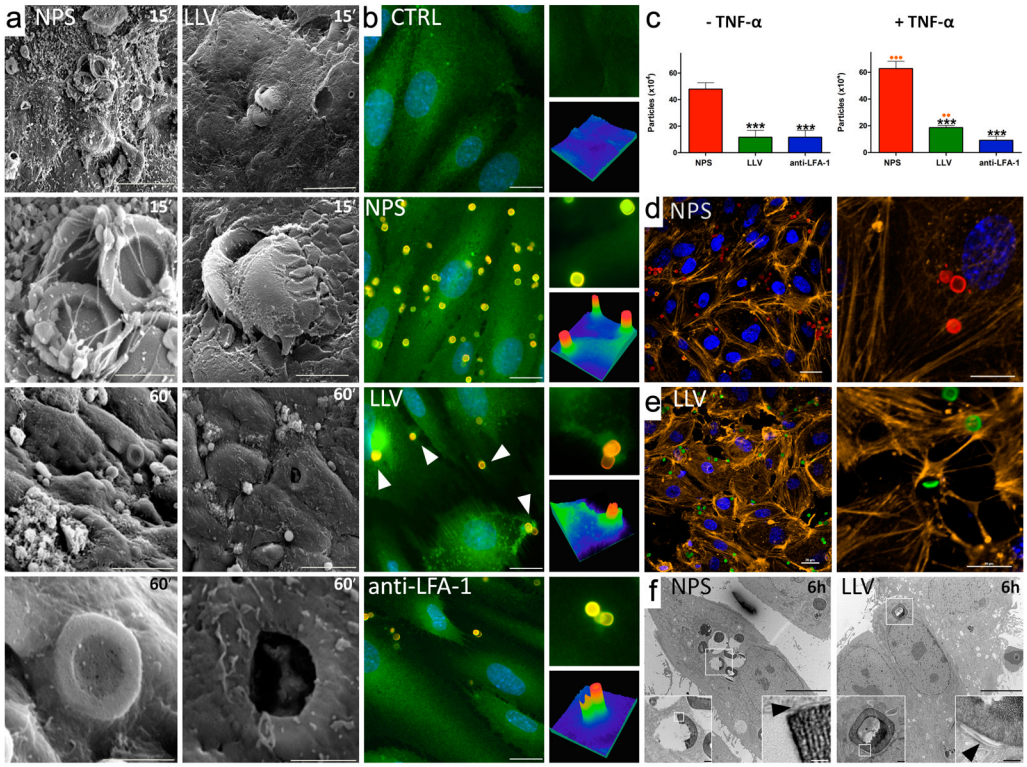

Figure 3. Particle adhesion to healthy and inflamed endothelium

a, SEM micrographs of NPS and LLV uptake by HUVEC cells pre-treated with TNF-α. Low and high magnifications are shown for each condition (scale bars = 10 and 2 μm respectively). **b,** After treatment with NPS, LLV, or LLV pre-incubated with anti-LFA-1 antibody (particles, yellow), ICAM-1 clusters (green, arrows) on particles at the surface of TNF-α stimulated HUVEC cells. High magnification images and colorimetric analysis of receptor clustering is shown to the right. Scale bars = 15 and 2 μm. **c,** Quantification of particle adhesion to normal (− TNF-α) and inflamed endothelium (+TNF-α) following 30 minutes of flow. ** = $p < 0.01$, *** = $p < 0.001$. Black asterisks identify significance between particle types while orange dots signal differences in TNF-α treated or untreated groups. **d–e**, Confocal microscopy of HUVEC treated with NPS (red) or LLV (green) for 3 hours show reorganization of actin filaments (orange). Scale bars = 20 and 10 μm. **f**, TEM micrographs of NPS or LLV 6 hours after particle addition show lysosomal sequestration and cytoplasmic accumulation (respectively) with high magnification images to the right. Scale bars = 10 μm, 2 μm, and 100 nm.

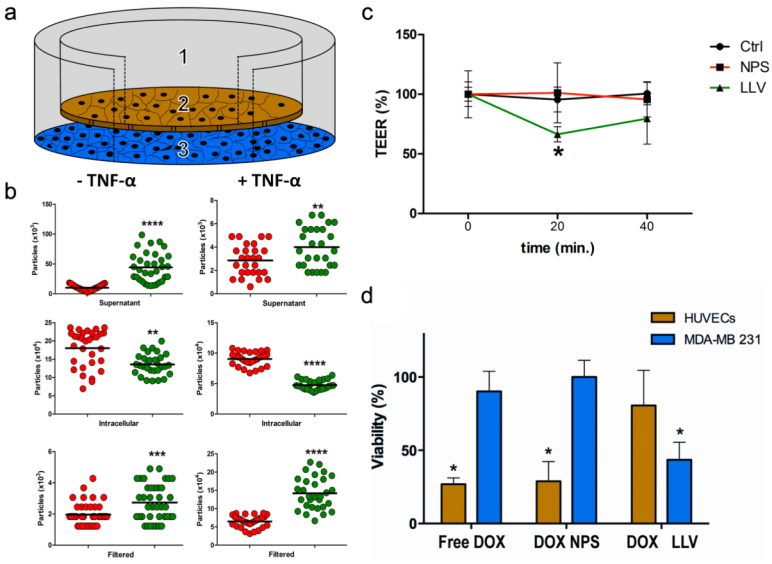

Figure 4. LLV effect on endothelial barrier function

a, Schematic of a transwell chamber for assaying transport across a cellular monolayer. Particles were counted in the upper chamber (1: supernatant), endothelial layer (2: intracellular), and lower chamber (3: filtered). **b,** Quantification of particle localization after 3 hours with or without TNF-α demonstrated significantly enhanced transport of LLV (green dots) compared to NPS (red dots). **c,** Evaluation of TEER, normalized against untreated controls. LLV were found to produce a transient decrease in TEER measurements of confluent inflamed endothelium. **d**, Studies of HUVEC (endothelial) and MDA-MB-231 (cancer) cell viability in a transwell system. LLV loaded doxorubicin (DOX LLV) showed enhanced tumour cell killing and decreased endothelial cell death following 48 hr incubation compared to free doxorubicin (Free DOX) and NPS loaded doxorubicin (DOX-NPS). * = $p < 0.05$, ** = $p < 0.01$, *** = $p < 0.001$, **** = $p < 0.0001$.

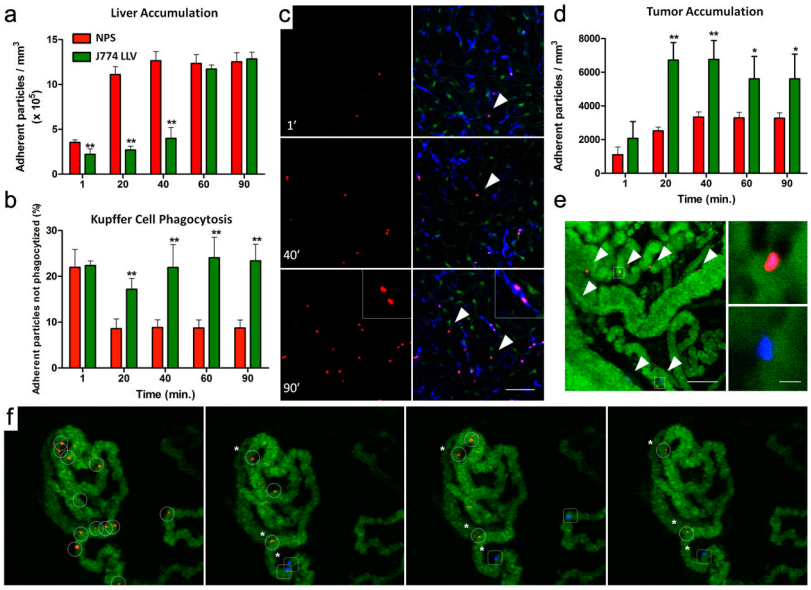

Figure 5. Enhanced tumoritropic accumulation in mice

a, Time-dependent accumulation of systemically administered J774-derived LLV and NPS particles in the liver of live mice. **b,** Time-dependent avoidance of phagocytosis displayed as the number of particles not associated with liver macrophages (Kupffer cells). **c,** Representative images of LLV (red) accumulation and uptake by Kupffer cells (blue) within the microvasculature (green) of healthy Tie-2 GFP+ mice, as measured by single-particle intravital microscopy (IVM). Phagocytized LLV are distinguished by a violet appearance in multicolour overlay images (see insets). Arrows indicate non-phagocytized LLV. Scale = 100μm. **d,** Time-dependent accumulation of systemically administered LLV and NPS in murine B16 melanoma tumours, as measured by single-particle IVM. **e,** Adhesion of individual LLV (red) and NPS (blue) particles, indicated by arrows, to the tumour endothelium (green), imaged and quantified 90 minutes after injection. High magnification images of boxes shown to the right. Scale = 100μm and 5μm. **f,** Representative images of circulating and adherent LLV (red, circles) and NPS (blue, squares) in the melanoma microvasculature (green). Asterisks indicate adherent particles. Scale bars = 100μm. * = $p<0.05$, ** = $p<0.01$, n=4.